Title

Non-invasively differentiating extent of liver fibrosis by visualizing hepatic integrin Î±vÎ²3 expression with an MRI modality in mice

Journal

Biomaterials, 102

ISSN

01429612

Authors

Li, Feng
Yan, Huihui
Wang, Jiyao
et al.

Publication Date

2016-09-01

DOI

10.1016/j.biomaterials.2016.06.026

Peer reviewed

Biomaterials 102 (2016) 162–174

Contents lists available at ScienceDirect

Biomaterials

journal homepage: www.elsevier.com/locate/biomaterials

Non-invasively differentiating extent of liver fibrosis by visualizing hepatic integrin αvβ3 expression with an MRI modality in mice

Feng Li [a, 1], Huihui Yan [a, b, 1], Jiyao Wang [a, c, *], Cong Li [d], Jian Wu [c, e], Shengdi Wu [a], Shengxiang Rao [f], Xihui Gao [d], Qu Jin [d]

[a] Department of Gastroenterology, Fudan University-Affiliated Zhongshan Hospital, Shanghai, China
[b] Department of Gastroenterology, The Second Affiliated Hospital, School of Medicine, Zhejiang University, Hangzhou, Zhejiang Province, China
[c] Shanghai Institute of Liver Diseases, Shanghai, China
[d] Key Laboratory of Smart Drug Delivery, Ministry of Education & PLA, School of Pharmacy, Fudan University, Shanghai, China
[e] Key Laboratory of Medical Molecular Virology, Ministries of Education and Public Health, Department of Medical Microbiology, Fudan University Shanghai Medical College, Shanghai, China
[f] Department of Radiology, Fudan University-Affiliated Zhongshan Hospital, Shanghai, China

ARTICLE INFO

Article history:
Received 30 January 2016
Received in revised form
20 May 2016
Accepted 13 June 2016
Available online 16 June 2016

Keywords:
Nanoprobe
Hepatic stellate cells
Integrin αvβ3
Liver fibrosis
MRI modality

ABSTRACT

Aims: To explore the potential of a dendrimer nanoprobe labeled with cyclic arginine-glycine-aspartic acid pentapeptide (cRGDyK) as a magnetic resonance imaging (MRI) tracer to non-invasively differentiate the extent of liver fibrosis.
Methods: Synthetic dendrimer nanoprobes were labeled with cRGDyK (Den-RGD) to form a formulation of hepatic stellate cell (HSC)-specific MRI tracer. An MRI modality was employed to visualize hepatic Den-RGD deposition in a mouse model of liver fibrosis caused by thioacetamide treatment.
Results: Den-RGD bound to activated HSCs via integrin αvβ3 receptors. The labeling of nanoprobes with cRGDyK increased their affinity to and accelerated their uptake by activated HSCs. Most of intravenously administrated Den-RGD nanoprobes deposited in the fibrotic areas, and the deposited amount was paralleled with the severity of liver fibrosis. Majority of cells taking-up Den-RGD was found to be activated HSCs in fibrotic livers. An MRI modality using Den-RGD as a tracer demonstrated that the relative hepatic T1-weighed MR signal value was increased in parallel with the severity of liver fibrosis.
Conclusion: The extent of Den-RGD deposition reflects integrin αvβ3 expression in activated HSCs, and Den-RGD appears to be a useful formulation of MRI tracer and may non-invasively and quantitatively assess the extent of liver fibrosis.

1. Introduction

Chronic liver disease (CLD) represents a substantial public health problem with mortality attributable to cirrhosis of around 800,000 deaths per year worldwide [1]. Prognosis and management of CLD largely depend on the severity and progression of liver fibrosis [1]. Hence, the assessment of liver fibrosis is pivotal for the management of patients with CLD. Liver biopsy has traditionally been considered as the gold standard for determining the severity of hepatic fibrosis. However, it is an invasive procedure, with a risk of rare but potentially life-threatening complications, and is also prone to sampling errors [2]. Additionally, for the treatment of CLD, one of the main therapeutic goals is to reverse hepatic fibrosis [3–5]. To monitor the dynamic feature of fibrotic progression and regression, one needs to quantitatively assess the severity of

Abbreviations: CLD, Chronic liver diseases; ECM, extracellular matrix; HSCs, hepatic stellate cells; RGD, arginine-glycine-aspartic acid; cRGDyK, cyclo[Arg-Gly-Asp-(D)Tyr-Lys]; MRI, magnetic resonance imaging; Den-RGD, the targeted nanoprobe labeled with cRGDyK; Den-PEG, the control nanoprobe without cRGDyK labeling; Mal, maleimide; NHS, N-hydroxysuccinimidyl; PEG, polyethylene glycol; DOTA, 1,4,7,10-Tetraazacyclododecane-1,4,7,10-tetraacetic acid; Gd, gadolinium; DAPI, 6-diamidino-2-phenylindole; TAA, thioacetamide; ROI, region of interest; ΔT1, the average value of the relative hepatic signal intensity; ALT, alanine aminotransferase.

* Corresponding author. Department of Gastroenterology, Fudan University-Affiliated Zhongshan Hospital, 180 Fenglin Road, Shanghai, 200032, China.
E-mail address: wang.jiyao@zs-hospital.sh.cn (J. Wang).
[1] These two authors contributed equally to this study.

http://dx.doi.org/10.1016/j.biomaterials.2016.06.026
0142-9612/

fibrotic deposition. Nevertheless, the quantitation of hepatic fibrosis in biopsied specimens with technologies such as morphometric analysis remains semi-quantitative [1,4,5]. Moreover, it is unpractical to repeatedly perform a liver biopsy procedure during a short-term follow-up due to the invasive nature of liver biopsy when the potential anti-fibrotic effect needs to be evaluated before and after a medication was administrated for several times [4,5]. Thus, it is essential to develop non-invasive methods that are sensitive enough to visualize minor changes of fibrosis. Unfortunately, none of the current non-invasive approaches has reached this degree of sensitivity [4–7].

Liver fibrosis is a result of excessive extracellular matrix (ECM) deposition in response to chronic inflammatory injury, which is determined by a dynamic balance between ECM production and degradation. Myofibroblasts, representing a spectrum of ECM-producing cells that mainly derive from hepatic stellate cells (HSCs) and portal fibroblasts, are the major producers of ECM and are considered to be the most critical cellular effectors of liver fibrosis [3].

Integrins are a large family of heterodimeric cell surface receptors composed of non-covalently linked α- and β-subunits, which act as mechanoreceptors by relaying the signals between ECM and cells, or between different cells [8]. It has been found that integrin αvβ3 is expressed by HSCs during their activation *in vitro*, and promotes HSCs proliferation and survival [9]. More importantly, it has been observed that hepatic expression of integrin αvβ3 is markedly up-regulated in rats with liver fibrosis, and positively correlated to the stages of fibrotic progression [10,11].

Many integrins recognize a common motif in their ligands. One of best characterized motifs is the arginine-glycine-aspartic acid (RGD) sequence. The integrin-binding activity of adhesion ligands can be reproduced by short synthetic peptides containing this motif [12]. In the previous studies, it has been demonstrated that a synthesized cyclic RGD pentapeptide (cyclo [Arg-Gly-Asp-(D)Tyr-Lys], cRGDyK) binds to both purified and membrane-bound integrin αvβ3 receptor on activated HSCs with a high affinity in a reversible fashion [13].

Among the multiple imaging modalities used in clinic, magnetic resonance imaging (MRI) shows the highest spatial resolution to soft tissues (up to 200 μm) and is especially useful to distinguish small lesions. In the present study, we labeled a well-characterized dendrimer with cRGDyK to formulate an integrin αvβ3-targeted nanoprobe. With this novel nanoprobe as a tracer, we successfully developed a non-invasive MRI modality to quantitatively assess the extent of liver fibrosis by imaging hepatic integrin αvβ3 expression in mice.

2. Materials and methods

2.1. Materials

All organic solvents were analytical grade from Aladdin Reagent (Shanghai, China) unless otherwise specified. Fmoc-Gly-2-cl-Trt resin was purchased from Applied Biosystems (Carlsbad, California, USA). Polyamidoamine (PAMAM) G5 dendrimer (77.35 mg/mL in methyl alcohol, containing 128 primary amino groups, MW: 28,826 Da) was purchased from Dendritech Inc (Midland, MI, USA). Rhodamine succinimide ester was purchased from Thermofisher scientific (NY, USA). Activated polyethylene glycol (PEG) derivatives, Malemide-PEG^{2k}-NHS ester and PEG^{2K}-NHS ester were purchased from JenKem Technology Co. Ltd (Beijing, China). 1,4,7,10-Tetraazacyclododecane-1,4,7,10-tetraacetic acid (DOTA)-NHS ester was purchased from Macrocyclics (TX, USA). $Gd_2(CO3)_3$, DNase I, Nycodenz, 6-diamidino-2-phenylindole (DAPI) and Bolton-Hunter reagent were purchased from Sigma-Aldrich (St. Louis, MO, USA). Collagenase NB4 (standard grade) was purchased from SERVA (Heidelberg, Germany). Pronase E was purchased from Roche (Basel, Switzerland). Isoflurane (AERRANE) was purchased from Baxter Healthcare Corporation (New Providence, NJ, USA). Fetal bovine serum, penicillin and streptomycin, high glucose DMEM, Alexa Flour 488-labeled donkey anti-mouse secondary antibody, Alexa Flour 488-labeled rat anti-mouse secondary antibody, Alexa Fluor 488-labeled goat anti-rat secondary antibody, Alexa Flour 488-labeled donkey anti-goat secondary antibody and Alexa Flour 488-labeled goat anti-rabbit secondary antibody were purchased from Invitrogen (Carlsbad, CA, USA). Rabbit anti-mouse α-SMA antibody, rat anti-mouse CD68 antibody and rat anti-mouse CD31 antibody were purchased from Abcam (MA, USA). Rabbit anti-mouse integrin β3 antibody was purchased from Epitomics (Burlingame, CA, USA). Goat anti-mouse CD163 antibody was purchased from SANTA CRUZ Biotechnology INC. (CA, USA).

2.2. Experimental animals

C57BL/6J mice were purchased from the Department of Experimental Animals, Fudan University, and housed in a specific pathogen-free facility. The experimental design and procedures were approved by the Institutional Ethical Committee of Animal Experimentation, and all experiments were performed strictly according to governmental and international guidelines on animal experimentation.

2.3. Synthesis, formulations and characterization of nanoprobes

The targeted dendrimer nanoprobe labeled with cRGDyK (referred to as Den-RGD) and the control dendrimer nanoprobe without cRGDyK labeling (referred to as Den-PEG) were prepared as described previously [13,14]. Briefly, cRGDyK was firstly synthesized by an Fmoc-protected solid-phase peptide synthetic method. Then, dendrimers in the fifth generation (PAMAM G5 dendrimer) were chosen as the platform of the nanoprobe preparation, given that this dendrimer (diameter: 7 nm) possesses a prolonged blood circulation time compared to low generation dendrimers and is excreted from both renal and hepatobiliary systems [15]. In Den-RGD, the cRGDyK peptide was labeled onto the dendrimer surface through a flexible PEG linkage. Both Den-RGD and Den-PEG were modified with rhodamine fluorophores and paramagnetic Gd-DOTA chelators. The synthesis processes were illustrated in Fig. 1.

The characteristics of nanoprobes were measured as previously described [13,14]. In brief, the molar ratio between dendrimer, PEG, cRGDyK and DOTA was quantified by measuring the proton integration of dendrimer (3.3–2.2 ppm), PEG (3.7 ppm, O-CH_2), cRGDyK (7.2–6.7 ppm) and DOTA (3.3–2.2 ppm) in the ^{1}H NMR spectrum. The labeling proportion of rhodamine was determined by measuring the absorbance of rhodamine (ε_{552} = 60,000 M^{-1} cm^{-1}) according to Lambert-Beer's law: A = lg (1/T) = Kbc (A: absorbance, T: transmission factor, c: concentration, b: thickness of the absorber) by UV-2401PC UV–vis Recording spectrophotometer (SHIMADZU, Kyoto, Japan). The molecular weight of nanoprobes was determined by MALDI-TOF MS, which was conducted using an AB SCIEX TOF/TOF™ 5800 mass spectrometer (Applied Biosystems, CA, USA). The hydrodynamic radius of nanoprobes and unmodified G5 dendrimer were determined by a Malvern Zetasizer (Malvern Instruments Inc., Southborough, MA) and dynamic light scattering instrument (DLS) at room temperature. In order to determine the surface charges of nanoprobe, the instrument was calibrated with the standard solution with a Zeta potential of −50 mV. The Gd^{3+} concentration of nanoprobe was determined by a Hitachi P-4010 (Tokyo, Japan) ICP-AES (Inductively Coupled Plasma Atomic Emission Spectroscopy) system with RF power at 1100 W and nebulizer gas flow at 0.9 L/min. The longitudinal relaxivity of the nanoprobes and the commercial available MR contrast agent Gd^{3+}-DOTA were determined on a

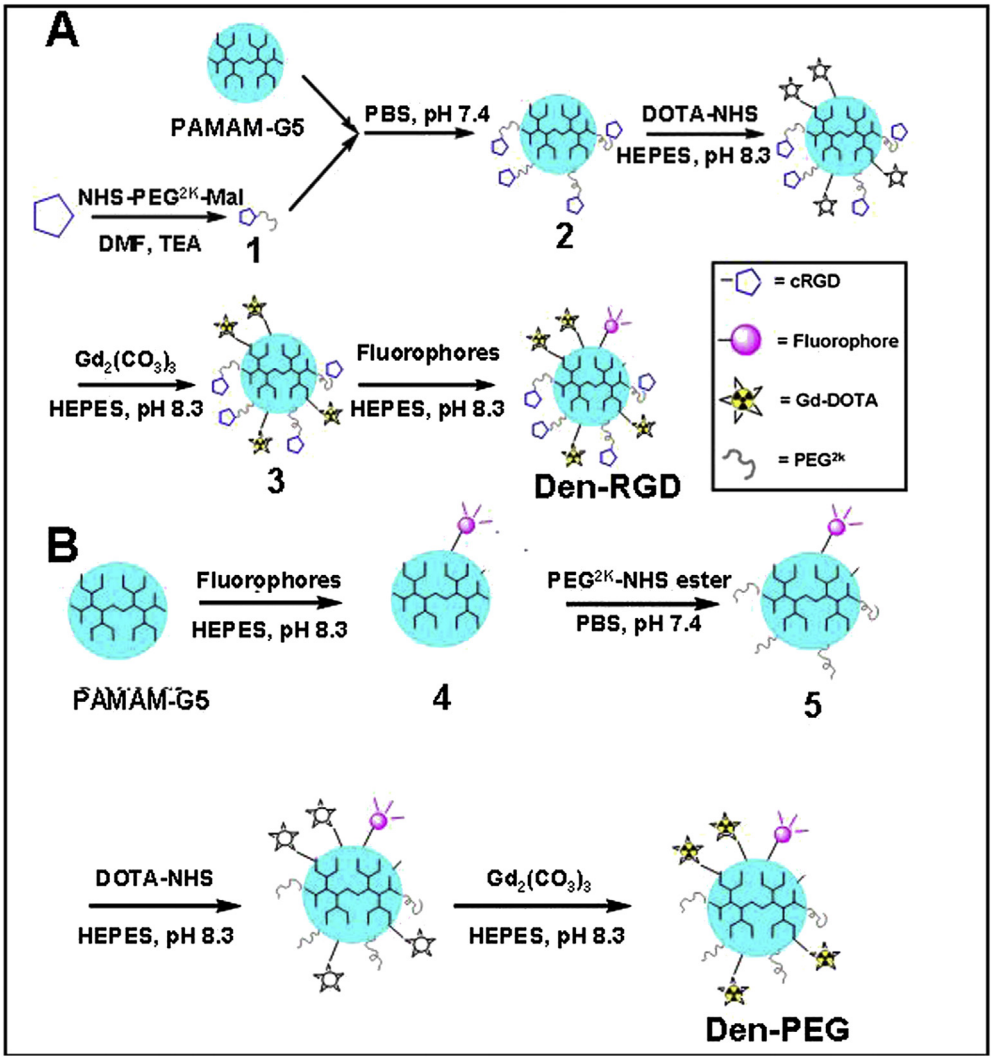

Fig. 1. Schematic illustration of synthetic steps of the targeted nanoprobe Den-RGD (A) and the control nanoprobe Den-PEG (B). (A) For the formulation of Den-RGD nanoprobes, treatment of maleimide (Mal) and N-hydroxysuccinimidyl (NHS) ester-functionalized PEG derivative Mal-PEG^{2K}-NHS with cRGDyK offered compound #1, which further reacted with G5 dendrimer (PAMAM-G5) to give compound #2. The conjugation of DOTA-NHS ester and $Gd_2(CO_3)_3$ with compound #2, respectively, gave compound #3, which was then complexed with rhodamine-NHS ester to produce Den-RGD. **(B)** To prepare Den-PEG, G5 dendrimer was firstly complexed with rhodamine-NHS eater to give compound #4, which further reacted with PEG^{2K}-NHS ester to give compound #5. Then, the conjugation of DOTA-NHS ester and $Gd_2(CO_3)_3$ with compound #5, respectively, produced Den-PEG. DMF, dimethyl formamide; TEA, Tri Ethyl Amine; HEPES, 2-hydroxyethyl; PBS, phosphate buffer solution.

Bruker Biospec 47/30 MRI scanner according to the equation of $r_{1p} = (1/T_{sample} - 1/T_{PBS})/[Gd]$. The T values of PBS and selected compounds with four different concentrations in PBS (pH 7.4) were measured with a 4.7 T MR spectrometer at 25 °C.

2.4. Isolation and culture of HSCs

Mouse HSCs were isolated by enzymatic digestion and Nycodenze density gradient centrifugation [16], and cultured in high glucose DMEM supplemented with 10% fetal bovine serum and antibiotics at 37 °C. After being cultured for 7 days, primary HSCs showed the characteristics of myofibroblasts, and they were designated as activated HSCs and used for further experiments.

2.5. Affinity of Den-RGD nanoprobes to activated HSCs

After being detached by trypsin digestion, activated HSCs were seeded on 35 mm glass bottom dishes and cultured to approximately 50% confluence. And then they were incubated with 2 mL of solution containing 4 μmol/L nanoprobes for 15 min at 4 °C, and for 2 or 24 h at 37 °C. After incubation, the cells were washed and imaged immediately by a confocal fluorescent microscope (Leica Inc., Wetzlar, Germany). For competitive studies, HSCs were pre-incubated with cRGDyK solution (80 μmol/L) for 30 min at 4 °C, then washed and incubated with Den-RGD solution (4 μmol/L) for 15 min at 4 °C.

2.6. Flow cytometry analysis

Activated HSCs were respectively incubated with 2 μmol/L of nanoprobe solution for 15, 30 min, 1, 4 or 24 h. After incubation, the cells were washed by centrifugation at 1776 g in 4 °C, fixed with 4% paraformaldehyde and analyzed immediately for up-take rate by BD FACSAria flow cytometer (Becton, Dickinson and Company, NJ, USA) in a quantitative fashion.

2.7. Cytotoxicity studies

The viability of activated HSCs treated with the nanoprobes was determined by an MTT cell proliferation assay, and the unmodified

G5 dendrimer was used as the control. Culture-activated HSCs were trypsinized and a single-cell suspension was obtained. Then, the cell suspension was added to 96-well plates (2×10^3 cells/well). After cultured for 24 h, cells were incubated with the nanoprobe solution or the unmodified G5 dendrimer solution with final concentrations in a range of 0.05–10 μmol/L. After being incubated for 4 days at 37 °C, cells were washed with PBS, and the cell viability was determined by MTT assay. The IC_{50} value was defined as the concentration of nanoprobes which could reduce cell viability by 50% using un-treated cells as a control.

2.8. Immunofluorescent localization of Den-RGD in HSCs

Activated HSCs were seeded on plastic dishes (2000/cm^2), and cultured overnight at 37 °C. They were washed with Tris–HCl buffer (20 mmol/L, pH 7.4), incubated with Den-RGD (4 μmol/L) solution for 2 h at 37 °C in the dark, and washed with Tris–HCl buffer at 4 °C. Then, rabbit anti-mouse integrin β3 antibody (1:200) and Alexa Flour 488-conjugated secondary antibody (1:200) were used for the visualization of integrin αvβ3 with DAPI for nuclear counter-staining (1:2,000). Multicolored fluorescent staining was visualized with a Leica TCS SP5 confocal laser-scanning microscope (Leica Inc., Wetzlar, Germany).

2.9. Animal model of liver fibrosis

C57BL/6J mice were injected with thioacetamide (TAA) intraperitoneally (200 mg/kg) for 4, 8 or 12 weeks three times per week, and these mice are referred to as TAA-4w, TAA-8w and TAA-12w. Mice treated with 0.9% sodium chloride served as a control group. Mice were subjected to the following experiments one week after the last injection to avoid acute effects of TAA.

2.10. Biodistribution of isotope-labeled nanoprobes

Nanoprobes were radiolabeled with iodine-125 (^{125}I) by the Bolton-Hunter (BH) method. Briefly, 9.0 μL of a fresh BH solution in benzene (0.36 g/L) was reacted with 1.0 mCi Na^{125}I and 20 μL chloramine-T (2.5 g/L in 0.05 mol/L phosphate buffer). After incubation for approximately 15 s, 10 μL sodium metabisulfite (12 g/L in 0.05 mol/L phosphate buffer), 10 μL NaI (20 g/L in 0.05 mol/L phosphate buffer) and 2 μL dimethylformamide were added and the above mixture was oscillated for 10 s. Next, the radiolabeled BH was immediately extracted with 0.5 mL benzene, transferred into a 1.5 mL centrifuge tube and dried under nitrogen. Finally, 2.4 mCi of ^{125}I-BH was obtained. For the radiolabeling of Den-RGD or Den-PEG, 0.5 mL nanoprobe (4.0 g/L in borate buffer, pH 8.0) was added to the dry ^{125}I-BH in a centrifuge tube under the protection of nitrogen, and the mixture was incubated for 30 min in an ice bath to obtain the final product. The product was further purified by using a Sephadex G25 gel column chromatography.

Both control and TAA-8w mice were injected respectively with [^{125}I]-labeled Den-RGD (200 μL, 8 μCi) or Den-PEG through the tail vein. The mice were sacrificed 2 or 24 h after injection (n = 3 per group). The heart, lungs, liver, spleen, kidneys, muscle and brain were excised, washed in saline and weighed. The radioactivity (cpm) of tissue homogenate was determined with an automatic scintillation counter. The total radioactivity in each organ was calculated and corrected for the blood-derived radioactivity. The biodistribution of [^{125}I]-labeled nanoprobes was calculated as a percentage of the injected dose per gram of wet tissue mass (%ID/g).

2.11. Autoradiographic imaging of liver tissue

Mouse livers were embedded in optimum cutting temperature compound, snap-frozen in liquid nitrogen and cryo-sectioned with a thickness of 15 μm after biodistribution study. The autoradiogram films were developed against separate liver sections by Leica MZ75 high-performance stereomicroscope (Leica Inc., Wetzlar, Germany). The autoradiographic images were collected by Perkin Elmer precisely storage phosphor system cyclone plus (Perkin Elmer, MA, USA), and the mean net gray scale intensity of each region of interest (ROI) was calculated.

2.12. In vivo MRI studies

In vivo MRI was performed in mice at 7.0 T using a Biospec 70/20 MRI scanner (Bruker Inc., Billerica, MA). Control mice and TAA-treated mice (n = 4) were subjected to the MR images to assess liver fibrosis at different stages after being injected with Den-RGD at a dose of 0.05 mmol/kg [Gd^{3+}] in a total of 0.25 mL of PBS solution.

In the process of MR imaging, isoflurane (0.5–2%) in 100% oxygen was inhaled upon the placement of mouse in the MR coil, and continuously adjusted by monitoring the respiration. The body temperature of the mouse within the magnet device was maintained by a thermostat-regulated heating pad, and the respiration was continuously monitored by a Bruke PhysioGard system. The gating device was used to reduce the interference of respiration to hepatic MR image. The tail vein was cannulated for intravenous administration of nanoprobes.

Dynamic T1-weighed images of the liver were collected prior to and 5, 30, 60, 90 and 120 min after injection. After a series of imaging, mice were returned to their cages and imaged again 24 h later. Coronal section images of the liver with 1 mm thickness were acquired with an MSME sequence (TR = 300 ms, TE = 11 ms, and number of average = 4), and 3D T1-weighed images were recorded with a fast low-angle shot (FLASH) sequence (flip angle = 45°, FOV = 2.3 cm × 2.0 cm × 2.3 cm, matrix size 128 × 128 × 33, TR = 35 ms, TE = 6.2 ms, and number of averages = 8). The signal intensity of hepatic region (T1 (liver)) in MR images was measured by eFilm Workstation 1.5.3 software, and the muscle signal intensity (T1 (muscle)) in the same sections was used to normalize the hepatic signal intensity, which was denoted as the relative hepatic signal intensity = T1 (liver)/T1 (muscle). For every mouse, at each indicated time point, three T1-MR images with the maximum hepatic area were selected to respectively measure the signal intensity of liver and muscle, and the average value of the relative hepatic signal intensity (ΔT1) was calculated.

Additionally, the hepatic MR images with Den-RGD and the control nanoprobes (Den-PEG) were compared in TAA-8w mice (n = 4). For competitive studies, a 20-fold dosage of cRGDyK was injected intravenously to block the receptors 2 h before the administration of Den-RGD.

2.13. Histological analysis of hepatic fibrosis

At the end of MRI study, mice were sacrificed by drawing-out all the blood under anesthesia (1% pentobarbital sodium, 40 mg/kg, intraperitoneally). The livers were immediately removed and respectively processed for further analysis. After being fixed in neutralized formalin, liver sections were stained with hematoxylin and eosin (H&E) or Sirius red. Extent of liver fibrosis was semi-quantitatively scored by an experienced histologist who was blind to the experimental protocol according to the Isake staging criteria [17]. For a morphometric analysis of liver fibrosis, the Sirius Red staining (fibrotic) areas were measured as previously described [10].

In addition, liver hydroxyproline content and serum alanine aminotransferase (ALT) level were determined using commercially available assay kits (JianCheng, Nanjing, China) according to the manufacturer's instructions.

2.14. Ex vivo fluorescent imaging of Den-RGD in fibrotic liver tissue

Frozen liver specimens were cryo-sectioned at 10 μm thickness, and sections were visualized with a laser-scanning confocal microscope (Leica TCS SP5, Leica Inc., Wetzlar, Germany). Rhodamine was excited with a 543 nm wavelength laser beam, and fluorescent emission was detected by a photomultiplier tube using a 560 nm band-pass filter.

2.15. Immunofluorescent colocalization of nanoprobes in various cell types of fibrotic livers

Immunofluorescent staining was performed to reveal the localization of Den-RGD nanoprobes in various cell types after immunohistologic staining with integrin αvβ3 and hepatic cellular markers including α-SMA (activated HSCs), CD68 (macrophages), CD31 (vascular endothelial cells) and CD163 (Kupffer cells) in the liver of TAA-12w mice. Primary rabbit anti-mouse β3 antibody (1:200), anti-mouse α-SMA antibody (1:400), rat anti-mouse CD68 antibody (1:50), rat anti-mouse CD31 antibody (1:50) and goat anti-mouse CD163 antibody (1:50) were used. Alexa Flour 488-conjugated secondary antibodies (1:200) were used for fluorescent imaging. 1% Triton X-100 was used for permeabilization and DAPI was used for nuclear counterstaining when appropriate. Liver sections with multicolored fluorescent staining were analyzed as previously described [10], and the percentage of the merged region (yellow color) to the total Den-RGD deposition region (red color) in each section was calculated. Ten randomly selected amplifying fields (400×) in each section were assessed.

2.16. Statistical analysis

SPSS 16.0 statistical software (Chicago, USA) was used. Quantitative data were presented as the mean ± standard deviation (SD). Comparisons between any given groups were achieved by one-way analysis of variance (ANOVA), followed by least significant difference (LSD) test. In all comparisons, a p value < 0.05 was considered statistically significant.

3. Results

3.1. Physical properties of nanoprobes

The molecular weight of cRGDyK was 620.45 Da, and the molecular weight of Den-RGD and Den-PEG were estimated as 81 and 82 kDa, respectively. The hydrodynamic diameter of Den-RGD was determined as 13.2 nm, which was slightly larger than that of Den-PEG (11.5 nm). In average, rhodamine was combined in a ratio of 1.4 to 1 Den-RGD; whereas it was bound to Den-PEG in a ratio of 1.5 to 1. The molar ratio of cRGDyK/DOTA/dendrimer in Den-RGD was 5/50/1, and the Gadolinium concentration in Den-RGD was 9.6%, which was lower than that in Den-PEG (12.5%). PEG was conjugated in a ratio of 5 to 1 Den-RGD and in a ratio of 7 to 1 Den-PEG. A T1-weighed longitudinal relaxivity value of both nanoprobes is in a range of 7.1–7.4 mM^{-1} s^{-1} (Table 1).

Table 1
Physical parameters of nanoprobes.

Nanoprobe	d (nm)	PDI	ζ(mV)	Gd %	r_{1p} (mM^{-1} s^{-1})	MW (kDa)
Den-RGD	13.2	0.193	10.4	9.6	7.1 ± 0.3	81
Den-PEG	11.5	0.109	16.7	12.5	7.4 ± 0.4	82
G5-Den	7.1	0.057	21.5	–	–	30

Diameters (d), polydispersity index (PDI), and zeta potentials (ζ) were measured by dynamic light scattering. Gadolinium concentration (Gd %) was measured by inductively coupled plasma atomic emission spectroscopy. T1-weighed relaxivity (r_{1p}) was determined on 4.7 T MRI at 25 °C. Molecular weight (MW) was measured by MALDI-TOF MS. Den-RGD, the targeted nanoprobe; Den-PEG, the control nanoprobe; G5-Den, the fifth generation (G5) dendrimer.

3.2. Cellular uptake and localization of nanoprobes

The uptake of Den-RGD (labeled with rhodamine) by activated HSCs was determined by confocal microscopic imaging. The fluorescent signal was clearly visible in activated HSCs after being incubated with Den-RGD solution (4 μmol/L) at 4 °C. When HSCs were pre-incubated with cRGDyK solution before being incubated with Den-RGD, fluorescent signal was almost invisible within these cells (Fig. 2A). These results confirmed that excessive cRGDyK markedly blocked the uptake of Den-RGD by activated HSCs.

In addition, enhanced fluorescent intensity was observed in activated HSCs incubated with Den-RGD solution for 2 h at 37 °C. In contrast, when the cells were incubated with Den-PEG, very faint fluorescent signal was recorded (Fig. 2B). However, fluorescent signal was obvious in the cells incubated with either Den-RGD or Den-PEG for 24 h at 37 °C (Fig. 2C). These results indicated that the modification of nanoprobes with cRGDyK could accelerate the uptake of Den-RGD nanoprobes by HSCs.

The uptake rate of Den-RGD nanoprobes by activated HSCs was quantitatively determined by flow cytometry. Mean fluorescent intensity in cells incubated with Den-RGD was significantly higher than those incubated with Den-PEG at corresponding time points ($p < 0.01$) (Fig. 2D), indicating that Den-RGD had a higher affinity and endocytosed rate than Den-PEG in activated HSCs.

The cytotoxicity of Den-RGD nanoprobes was evaluated with an MTT assay. As shown in Fig. 2E, the cytotoxicity of both Den-RGD and Den-PEG nanoprobes was lower than the unmodified G5 dendrimer, because the IC_{50} value of both nanoprobes was much higher than 5 μmol/L; whereas the IC_{50} of the unmodified G5 dendrimer was less than 0.5 μmol/L. Additionally, with an increase in its concentration, Den-RGD significantly decreased the viability of activated HSCs, while Den-PEG didn't have a marked effect.

To co-localize the Den-RGD with integrin αvβ3, immunofluorescent staining was performed in activated HSCs. The localization of Den-RGD (red) was largely overlapped with integrin αvβ3 positive-staining (green) (Fig. 3).

3.3. Biodistribution of nanoprobes in fibrotic mice

The biodistribution of nanoprobes was evaluated in control and TAA-8w mice 2 or 24 h after intravenous injection of [^{125}I]-labeled nanoprobes. After TAA treatment for 8 weeks, mice showed marked fibrosis in the liver. Both Den-RGD and Den-PEG nanoprobes were mainly located in the liver, spleen and kidneys (Fig. 4A and 4B). There was no significantly difference in the deposition amount between Den-RGD and Den-PEG in normal control livers, but much more Den-RGD than Den-PEG nanoprobes were deposited in the fibrotic livers 2 and 24 h after intravenous injection as indicated by percentage of injected dose. Additionally, more Den-RGD nanoprobes were deposited in the fibrotic livers than in normal livers at 2 and 24 h ($p < 0.01$ for all comparisons). All of these results indicate that more Den-RGD than Den-PEG nanoprobes were deposited in fibrotic livers because of the higher distribution of Den-RGD in fibrotic livers, not because of the longer blood circulation.

3.4. Autoradiographic visualization of nanoprobes in liver sections

Hepatic autoradiographic visualization of [^{125}I]-labeled nanoprobes was determined after the completion of the biodistribution

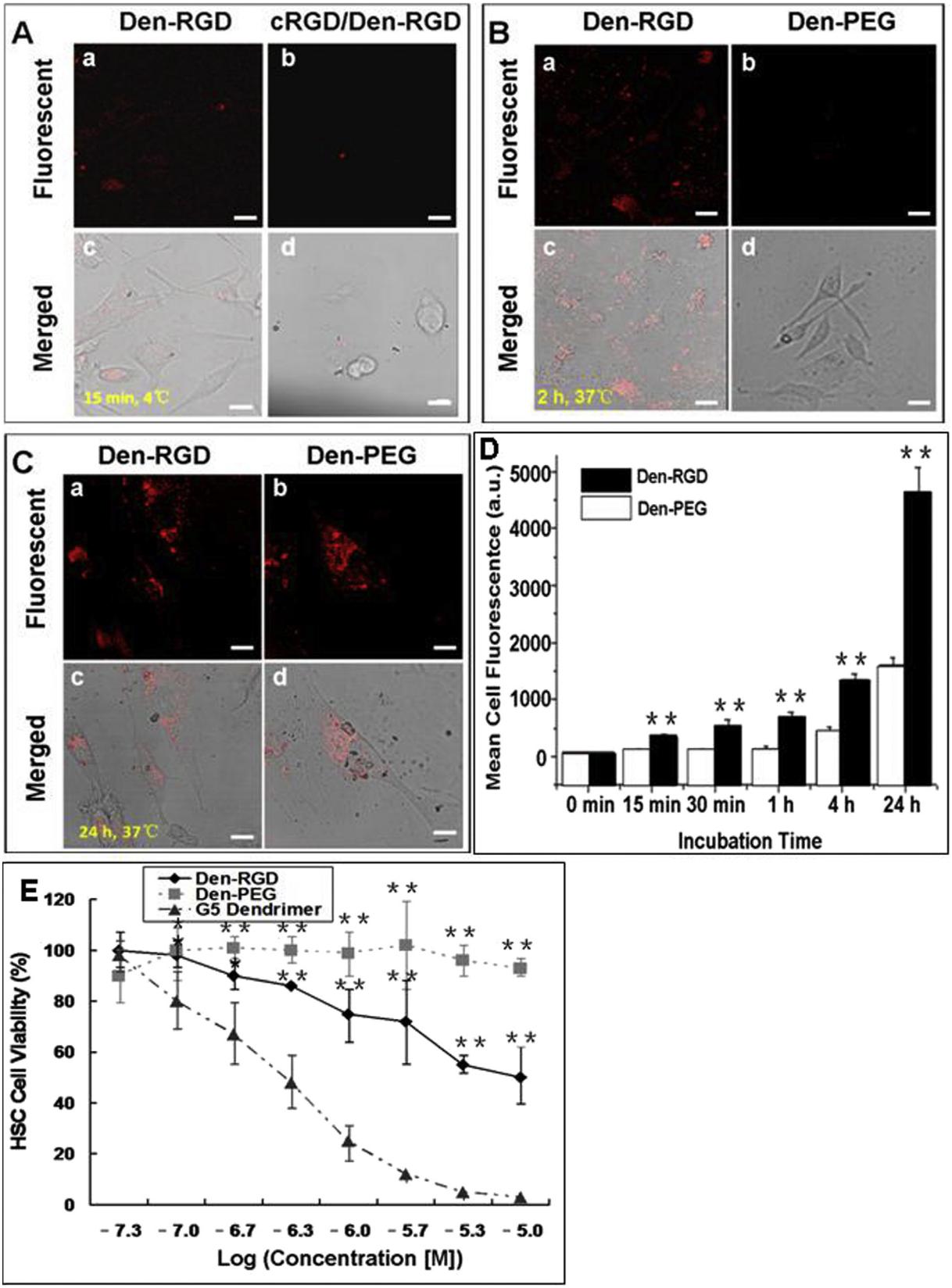

Fig. 2. Cellular uptake of nanoprobes in cultured-activated HSCs. (A) Imaging HSCs after incubation with Den-RGD or Den-RGD plus pre-incubation with excessive cRGDyK for 15 min at 4 °C. **(B, C)** Imaging HSCs after incubation with Den-RGD or Den-PEG for 2 or 24 h at 37 °C. Fluorescent images (a, b) and merged images (c, d) were taken at original magnification (400×). Scale bars, 100 μm. **(D)** Comparing the affinity of nanoprobes to activated HSCs by flow cytometry analysis at indicated time points. All experiments were undertaken in quintuplicates.**$p < 0.01$ compared to Den-PEG at corresponding time points. (**E**) Culture-activated HSCs were incubated with the nanoprobe solution or the unmodified G5 dendrimer solution at concentrations of 0.05–10 μM. After incubated for 4 days at 37 °C, cell viability was measured by MTT assay. All experiments were undertaken in triplicates. Data are expressed in means ± SD. *$p < 0.05$ versus G5 dendrimer; **$p < 0.01$ versus G5 dendrimer.

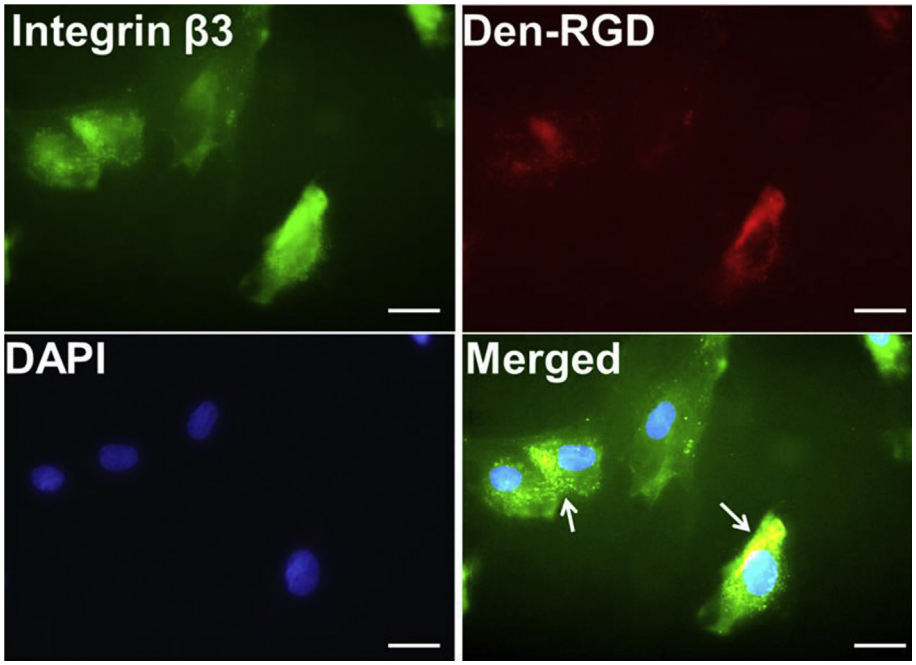

Fig. 3. Immunofluorescent localization of Den-RGD on activated HSCs. Representative fluorescent images of Den-RGD nanoprobes labeled with rhodamine (red color), counterstained with β3 integrin subunit antibody (green color) on culture-activated HSCs. DAPI was used for nuclei staining. The merged images show the yellow color areas pointed by white arrows. Images were recorded at original magnification (400×). Scale bars, 100 μm. (For interpretation of the references to colour in this figure legend, the reader is referred to the web version of this article.)

study. As shown in Fig. 4C, intensive radioactive signal was found in fibrotic liver sections, indicating that abundant Den-RGD nanoprobe was detected in the fibrotic livers. However, in normal liver sections, the radioactive signal was sparse, indicating less Den-RGD deposition. Compared to [^{125}I]-Den-RGD, hardly any [^{125}I]-Den-PEG nanoprobe was detected in both normal and fibrotic liver sections. By comparing radioactive intensity of ROI, much more [^{125}I]-Den-RGD than [^{125}I]-Den-PEG nanoprobe was detected in the fibrotic livers ($p < 0.01$), and more Den-RGD was detected in the fibrotic livers than in the normal livers ($p < 0.01$) (Fig. 4D).

3.5. Imaging of hepatic fibrosis with an MRI modality using Den-RGD as a tracer

A dynamic T1-weighed MR imaging approach was used to assess the deposition of Den-RGD in the livers after Den-RGD was intravenously injected in control and TAA-treated mice. As shown in Fig. 5A, there was no marked difference in hepatic signal intensity between control and TAA-treated mice before Den-RGD was injected; whereas hepatic signal intensity was significantly intensified in TAA-treated mice compared to control mice at 24 h post-injection, especially in TAA-12w mice for there was the strongest hepatic signal intensity. After Den-RGD was injected, ΔT1 in the control mice was quickly increased until 30 min post injection, then significantly decreased at 60 min post injection and further decreased after 120 min post injection. Until 120 min post injection, ΔT1 in TAA-treated mice was all gradually increased over time, and there was no significant difference among three groups. However 120 min post injection, ΔT1 was decreased in TAA-4w mice, slightly increased in TAA-8w mice and significantly increased in TAA-12w mice (Fig. 5B). Thus, the extent of liver fibrosis could be distinguished by comparing ΔT1 at 24-hrs time point post injection of Den-RGD. Compared to the pre-contrast value, ΔT1 at 24 h time point post injection was increased by 3.5 ± 6.0% in the control, 22.2 ± 2.6% in TAA-4w, 29.4 ± 0.26% in TAA-8w, and 36.3 ± 2.0% in TAA-12w groups ($p < 0.05$ for all comparisons), indicating that the deposition of Den-RGD reflected by ΔT1 at 24 h time point post injection was significantly increased with the development and progression of liver fibrosis.

The hepatic deposition of Den-RGD and Den-PEG nanoprobes was compared in TAA-8w mice. In TAA-8w mice injected with Den-PEG, ΔT1 was increased first and then gradually significantly decreased 60 min post injection. Compared to TAA-8w mice injected with Den-RGD, the pre-injection of cRGDyK significantly decreased ΔT1 90 min post injection (Fig. 5C). The similar results were also attained in TAA-4w and TAA-12w mice, but not in the control mice (data not shown).

3.6. Assessing the correlation of ΔT1 24 h post injection of Den-RGD nanoprobes with the extent of liver fibrosis

As shown by Sirius red-staining in Fig. 6A, fibrotic septa were gradually formed as the duration of TAA administration was prolonged, and extensive bridging-fibrosis in addition to a distortion of liver architecture was observed after TAA was administered for 12 weeks. The extent of liver fibrosis induced by TAA administration for 4, 8 and 12 weeks was respectively quantified with the Sirius red-staining (fibrotic) areas as 4.87 ± 0.59, 6.00 ± 0.43 and 11.65 ± 1.54% of the liver parenchyma area.

Next, we assessed the correlation between the extent of liver fibrosis and ΔT1 value 24 h after Den-RGD nanoprobes were injected. The ΔT1 at 24 h post injection showed a strong positive correlation with Ishake stage ($r = 0.815$, $p < 0.01$, Fig. 6B), Sirius red-staining area ($r = 0.842$, $p < 0.01$, Fig. 6C) or hydroxyproline content ($r = 0.781$, $p < 0.01$, Fig. 6D). These results indicated that hepatic deposition amount of Den-RGD 24 hrs after injection, which indicated by ΔT1, was gradually increased in parallel with the development and progression of liver fibrosis. However, there was no correlation between ΔT1 at 24 h post injection and ALT levels ($r = 0.371$, $p = 0.157$, Fig. 6E), which implied that hepatic

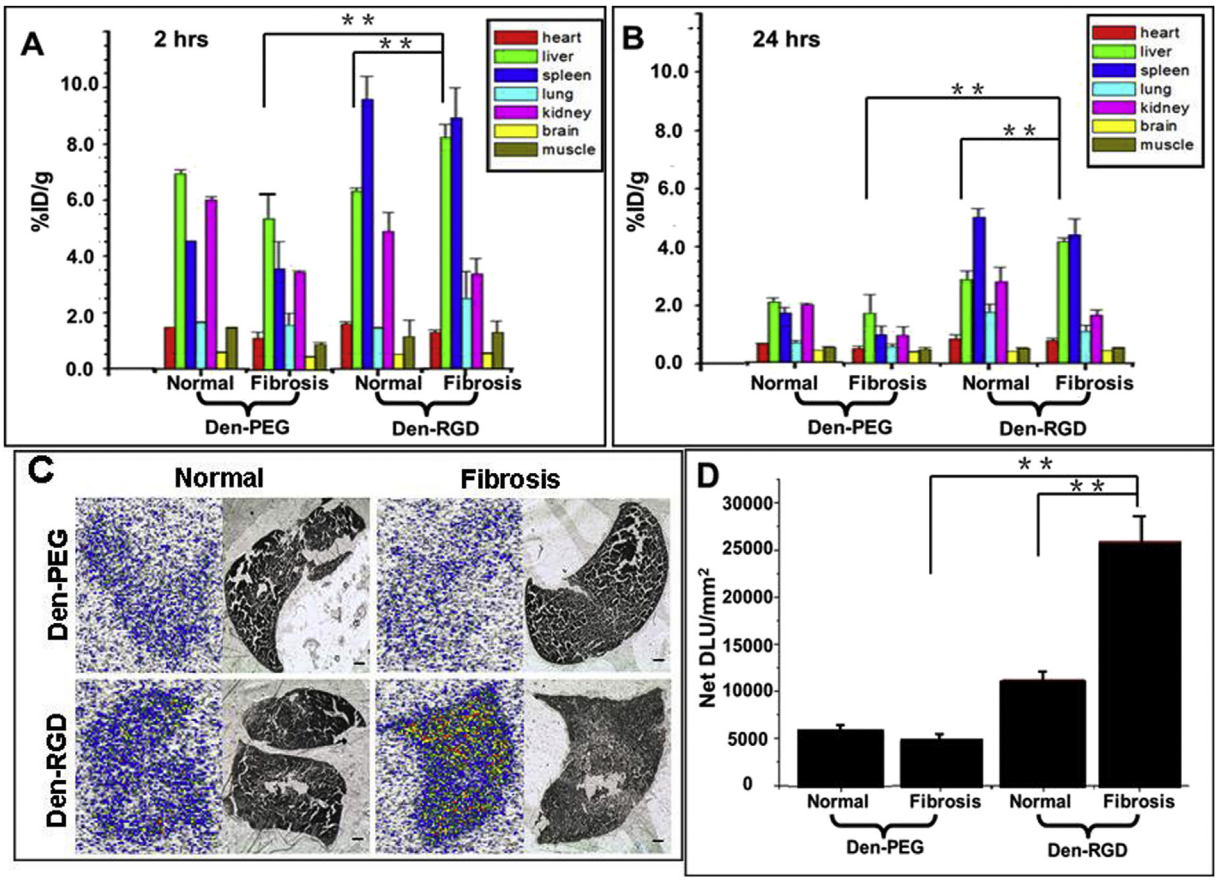

Fig. 4. Organ biodistribution and hepatic autoradiographic visualization of nanoprobes. (A, B) Organ bio-distribution was respectively determined in the control mice and the mice with liver fibrosis 2 h (A) and 24 h (B) after [^{125}I]-labeled Den-RGD or Den-PEG nanoprobes were injected. The organ accumulation amount of nanoprobes was compared (n = 3 per group). **(C, D)** Historadioautographic images of [^{125}I]-labeled nanoprobes in liver slices of the control and the mice with fibrosis. The autoradiogram images were collected (C) and the mean net gray scale (radioactive intensity: Net DLU/mm^2) was compared (D).**$p < 0.01$.

deposition amount of Den-RGD was not affected by hepatocyte injury.

3.7. Ex vivo fluorescent imaging of Den-RGD in liver sections

Because the nanoprobes were labeled with rhodamine, fluorescent imaging of Den-RGD and Den-PEG was performed in liver sections subsequently after MRI study. As shown by fluorescent imaging in Fig. 7, along with the progression of liver fibrosis, the fluorescent intensity became stronger in the liver sections than in normal livers after Den-RGD nanoprobe was injected, and was prominent only in the areas of fibrotic septa. The results indicated that Den-RGD nanoprobes were mainly deposited in the fibrotic area and the deposition amount was increased in parallel with the extent of liver fibrosis. Additionally, the fluorescent intensity in the liver sections of TAA-12w mice injected with Den-RGD nanoprobe was markedly stronger than that injected with Den-PEG nanoprobe, and was significantly reduced by the pre-injection of cRGDyK.

3.8. Localization of Den-RGD in fibrotic livers with immunofluorescent staining

In fibrotic livers, the localization areas of Den-RGD were found to be mainly overlapped with the positive-staining area of integrin β3 subunit (Fig. 8A), which indicated that the deposition of Den-RGD nanoprobes in fibrotic livers was highly possible to be mediated by integrin αvβ3 receptors.

The immunofluorescent staining was performed to further verify cell types that took-up Den-RGD in the fibrotic livers. After comparing the overlapped areas, it was found that the Den-RGD deposition area was largely overlapped with α-SMA positive-cells (43.1 ± 4.5%, Fig. 8B), and was partially overlapped with the CD31 (28.8 ± 4.4%, Fig. 8C) and CD68 positive-cells (18.2 ± 4.7%, Fig. 8D), but hardly was overlapped with CD163 positive-cells (2.6 ± 0.6%, Fig. 8E) ($p < 0.05$ for all comparisons, Fig. 8F). Because α-SMA is thought to be the marker of activated HSCs, the dominating cell types up-taking Den-RGD nanoprobes in the fibrotic livers are thought to be activated HSCs.

4. Discussion

Over the past decade, non-invasive methodologies, such as FibroTest or transient elastography (FibroScan), are in development to diagnose liver fibrosis, and they were validated as surrogates by liver biopsy [1,6,7]. Their usefulness as stage discriminators is becoming increasingly accepted, allowing the allocation of patients into three groups: no or minimum fibrosis, an intermediate stage and advanced fibrosis or cirrhosis [1]. However, patients in the intermediate stage, accounting for about 50% of CLD patients, would still need histopathologic examination to assess the extent of liver fibrosis. Thus, there is still an urgent need to develop non-invasive methods for reliable and quantitatively assess the extent of fibrosis. Compared to the non-invasive methodologies for the diagnosis of liver fibrosis currently used in clinic, this MRI modality

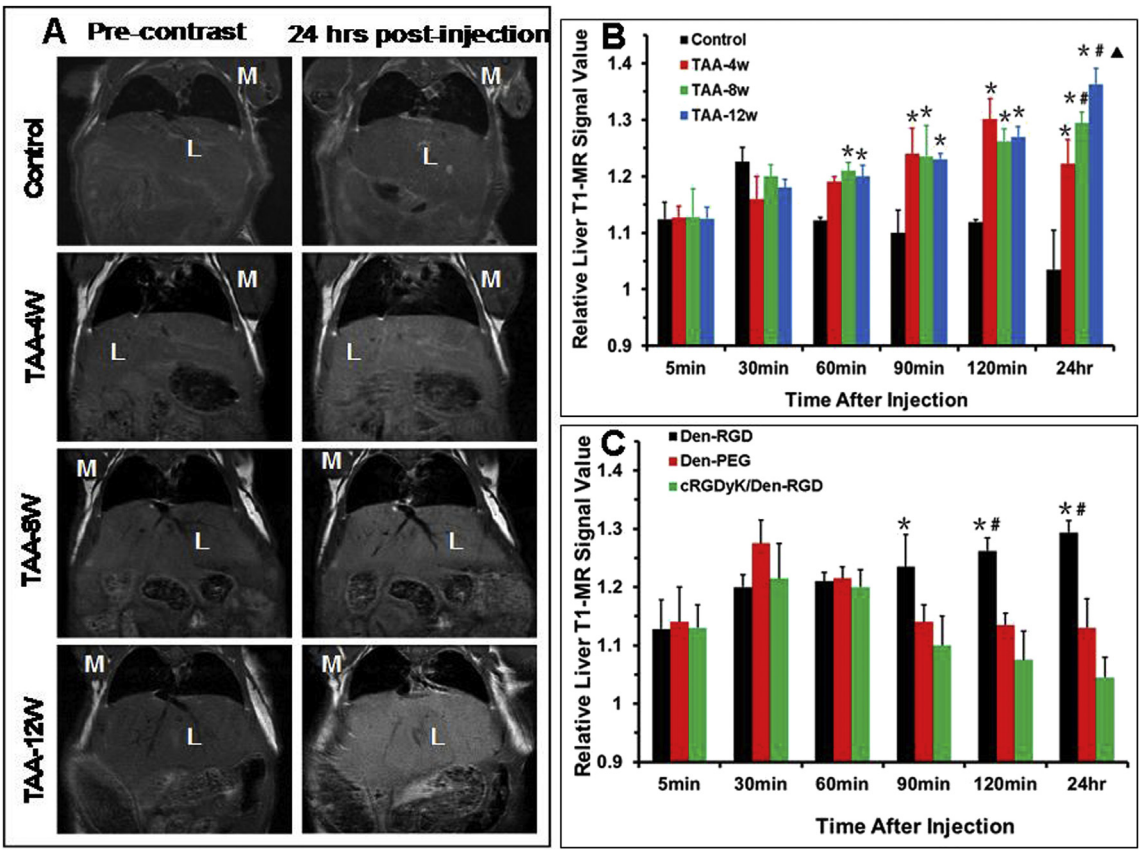

Fig. 5. Imaging liver fibrosis using an MRI modality with Den-RGD nanoprobes as a tracer in mice. (A) Representative hepatic T1-weighed MR images of the control and TAA-treated mice prior to and 24 h after Den-RGD injection were shown. L, liver; M, muscle. **(B)** Relative liver T1-MR signal value (ΔT1) in the control and TAA-treated mice was compared at corresponding time points after Den-RGD injection (n = 4). *$p < 0.05$ compared to the control mice; #$p < 0.05$ compared to TAA-4w mice; ▲ $p < 0.05$ compared to TAA-8w mice. **(C)** ΔT1 in TAA-8w mice was compared at corresponding time points after intravenous injection of Den-RGD, Den-PEG or Den-RGD plus pre-injection of excessive cRGDyK (n = 4). *$p < 0.05$ compared to mice injected with Den-RGD plus pre-injection of excessive cRGDyK; #$p < 0.05$ compared to mice injected with Den-PEG.

used in the study could directly image the change of fibrotic tissue in the whole liver, and even visualize the activity of HSCs during the development and progression of liver fibrosis. To our knowledge, there is no such a tracer commercially available for MRI imaging in the differentiating extent of liver fibrosis in clinical service and for animal experiment.

In rat models of liver fibrosis induced by bile duct ligation, TAA treatment or carbon tetrachloride treatment, hepatic integrin αvβ3 expression had been demonstrated to be positively correlated to the severity of liver fibrosis, which was increased with the development and progression of fibrosis and decreased with the regression of fibrosis [10]. Our findings were consistent with a study by Patsenker et al., that enhanced hepatic expression of integrin β3 subunit was positively correlated to the stage of fibrosis induced by bile duct ligation in rats [11]. In this context, it was convincing that the visualization of integrin αvβ3 expression in fibrotic livers would be likely to discriminate the extent of liver fibrosis.

Many radiolabeled-linear and cyclic RGD peptide antagonists have been evaluated as integrin αvβ3-targeted radiotracers to molecularly image tumor angiogenesis and metastasis [18]. It had also been shown that synthetic cyclic RGD peptides bind to integrin αvβ3 expressed on activated HSCs with an abundant receptor capacity and a high receptor-coupling affinity [10,13]. In the present study, the cyclic RGD peptide-labeled nanoprobe attained a selective binding to integrin αvβ3 receptors. The uptake of the targeted nanoprobes by activated HSCs was significantly inhibited *in vitro* by excessive cRGDyK. More importantly, in the MRI study, hepatic deposition of Den-RGD in the fibrotic livers, which was indicated by ΔT1, was markedly decreased by pre-administration of excessive cRGDyK. These results indicated that hepatic deposition of Den-RGD nanoprobes in fibrotic livers was mainly mediated by the receptor-coupling to cRGDyK. Moreover, the localization of Den-RGD nanoprobes on activated HSCs and in fibrotic livers was found to be mainly overlapped with the integrin αvβ3 positive-staining areas, where α-SMA-positive HSCs reside, indicating that Den-RGD deposition in the fibrotic livers was via coupling specifically to integrin αvβ3 on activated HSCs.

The major cell type expressing integrin αvβ3 in fibrotic livers has been found to be activated HSCs [10]. In the present study, in fibrotic liver, Den-RGD was found to mainly deposit in the areas of fibrotic septa by *ex vivo* fluorescent imaging study. And the deposition was largely overlapped with activated HSCs localization areas because the overlapped areas of Den-RGD deposition with α-SMA (activated HSCs marker)-positive area were significantly larger than that with other hepatic cellular markers. Thus, the majority of Den-RGD was presumably up-taken by activated HSCs. In addition to activated HSCs, integrin αvβ3 has also been reported to be expressed in vascular endothelial cells and inflammatory cells, especially monocytes and macrophages [19,20]. In the present study, we also observed that a smaller fraction of Den-RGD was uptaken by endothelial cells and macrophages, because the deposition area of Den-RGD was also overlapped in part with CD31 and CD68 positive-cells.

In the present study, Den-RGD nanoprobes were used as an MRI tracer, and Den-RGD deposition in the liver was reflected by hepatic T1-MR signal intensity. With the development and progression of

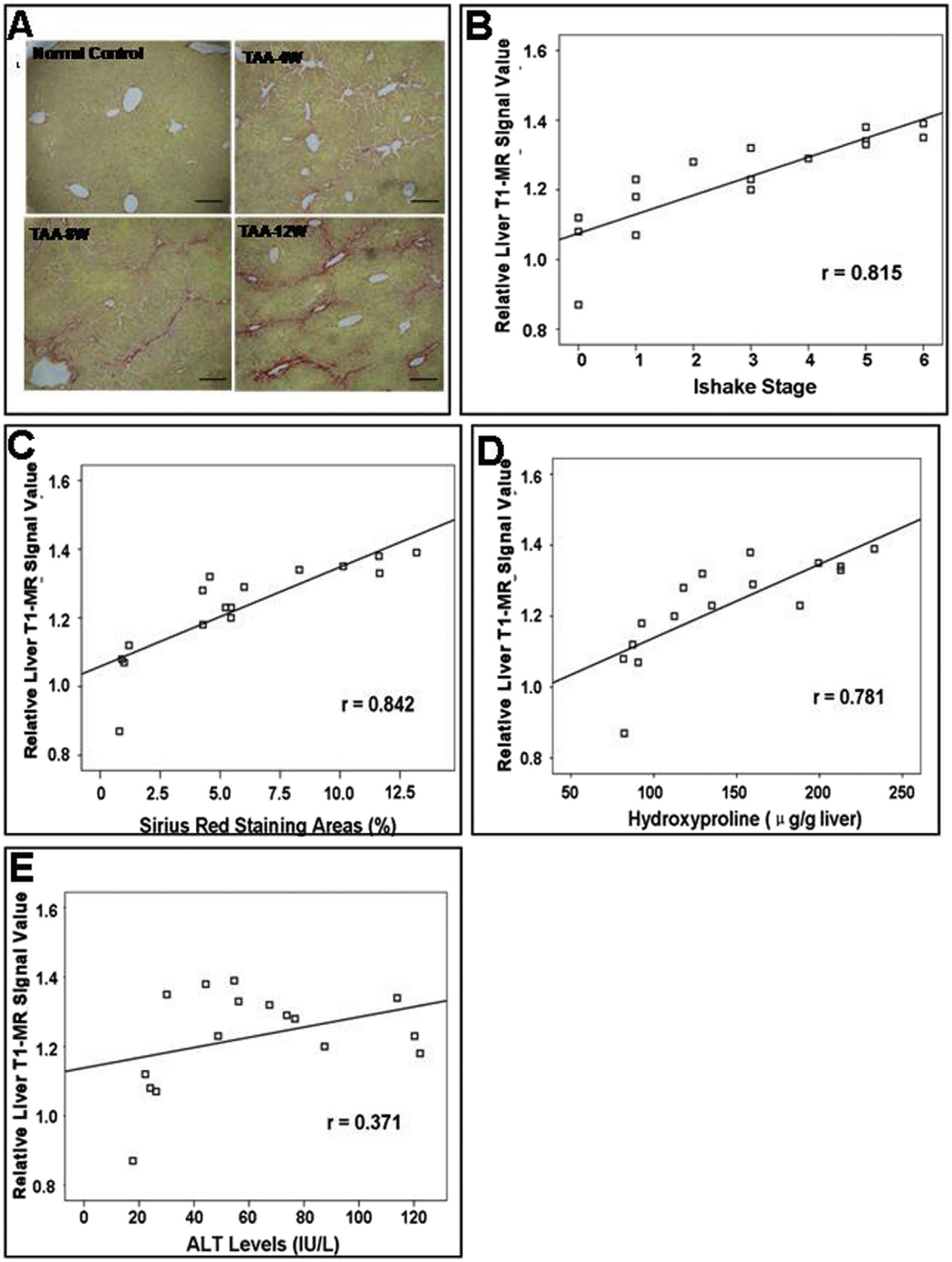

Fig. 6. Assessment of the correlation between ΔT1 at 24 h post-injection of Den-RGD nanoprobes and the extent of liver fibrosis. (**A**) Representative micrographs of hepatic histology stained with Sirius-red were shown. Images were taken at original magnification (100×). Scale bars, 100 μm. **(B–E)** The correlation of ΔT1 at 24 h post-injection of Den-RGD nanoprobes with Ishake stage (B), Sirius red-staining area (C), hydroxyproline content (D) and ALT levels (E) was assessed.

liver fibrosis, ΔT1 at 24 h post injection was found to be significantly increased, which indicates that more Den-RGD deposited in the livers with advanced fibrosis. More importantly, ΔT1 was found to be positively correlated with Ishake stage score, Sirius red-staining area and total collagen content as measured by hydroxyproline quantitation, all of which are semi-quantitative or quantitative and reflect the extent of liver fibrosis. Thus, the extent of liver fibrosis was successfully differentiated by reflecting hepatic deposition amount of Den-RGD. Because Den-RGD deposition in the fibrotic livers was via coupling specifically to integrin αvβ3, we claim that using Den-RGD nanoprobes as a novel tracer, we were able to non-invasively distinguish and quantitatively assess the

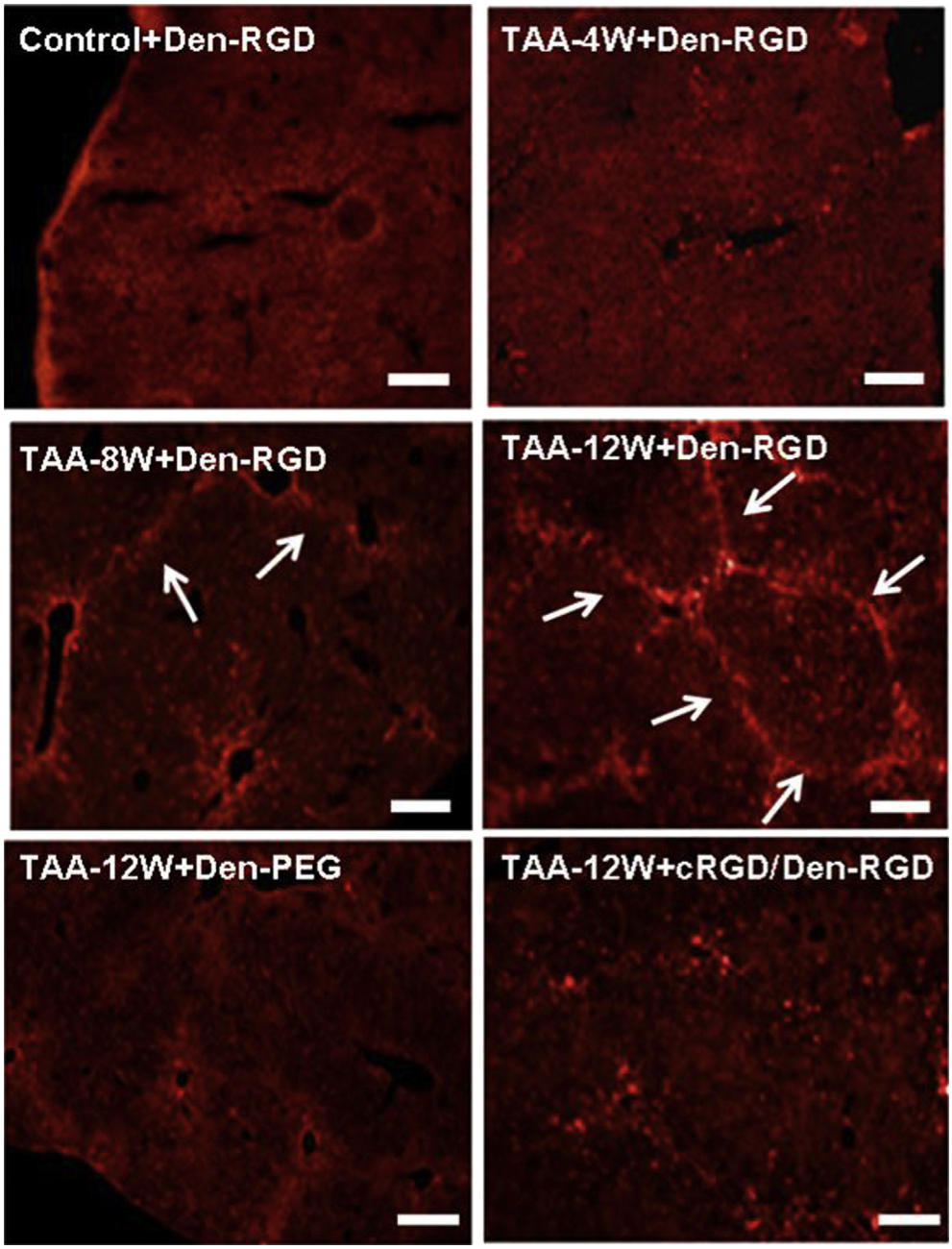

Fig. 7. ***Ex Vivo*** **Fluorescent Imaging of Den-RGD nanoprobes in Liver Sections**. Fluorescent imaging of hepatic sections was performed after MR imaging study, and representative images are shown. Images were recorded at original magnification (100×). Scale bars, 100 μm. The white arrows point to the deposition area of Den-RGD nanoprobes.

severity of liver fibrosis in mice by imaging hepatic integrin αvβ3 expression with an MRI modality.

In the previous study, we reported a non-invasive approach to distinguish different stages of liver fibrosis by imaging hepatic integrin αvβ3 expression with a SPECT modality in rats [10]. However, SPECT modality is incapable of imaging anatomical structure and the tracer is radioactive, both of which impede its clinical application. Compared to SPECT, the MRI modality possesses several outstanding advantages, such as 3-dimensional imaging capability, radioactivity-free and higher resolution [21]. Thus, in the present study, we developed an MRI modality to distinguish the extent of liver fibrosis with integrin αvβ3-targeted nanoprobes as a tracer. A new imaging modality by using MR technology to non-invasively stage liver fibrosis, called as magnetic resonance elastography, has been demonstrated to have a high accuracy for the diagnosis of advanced fibrosis and cirrhosis, independent of body mass index and etiology of CLD [22]. Additionally, a non-invasive method of fibrosis assessment by molecular MRI with a probe targeted to type I collagen was reported and is still in a preclinical stage [23,24]. The approaches of these modalities are different from ours which aims to develop a useful tracer of MRI modality for the diagnosis of liver fibrosis for patients with CLD.

As a novel drug carrier, the dendrimer may be modified by conjugating different imaging molecules in a targeting fashion on its surface so that it can achieve good targeted effect and high imaging sensitivity. The dendrimer possesses several advantages including its globular architecture, identical molecular weight, optimized circulation lifetime and well-defined reactive groups on

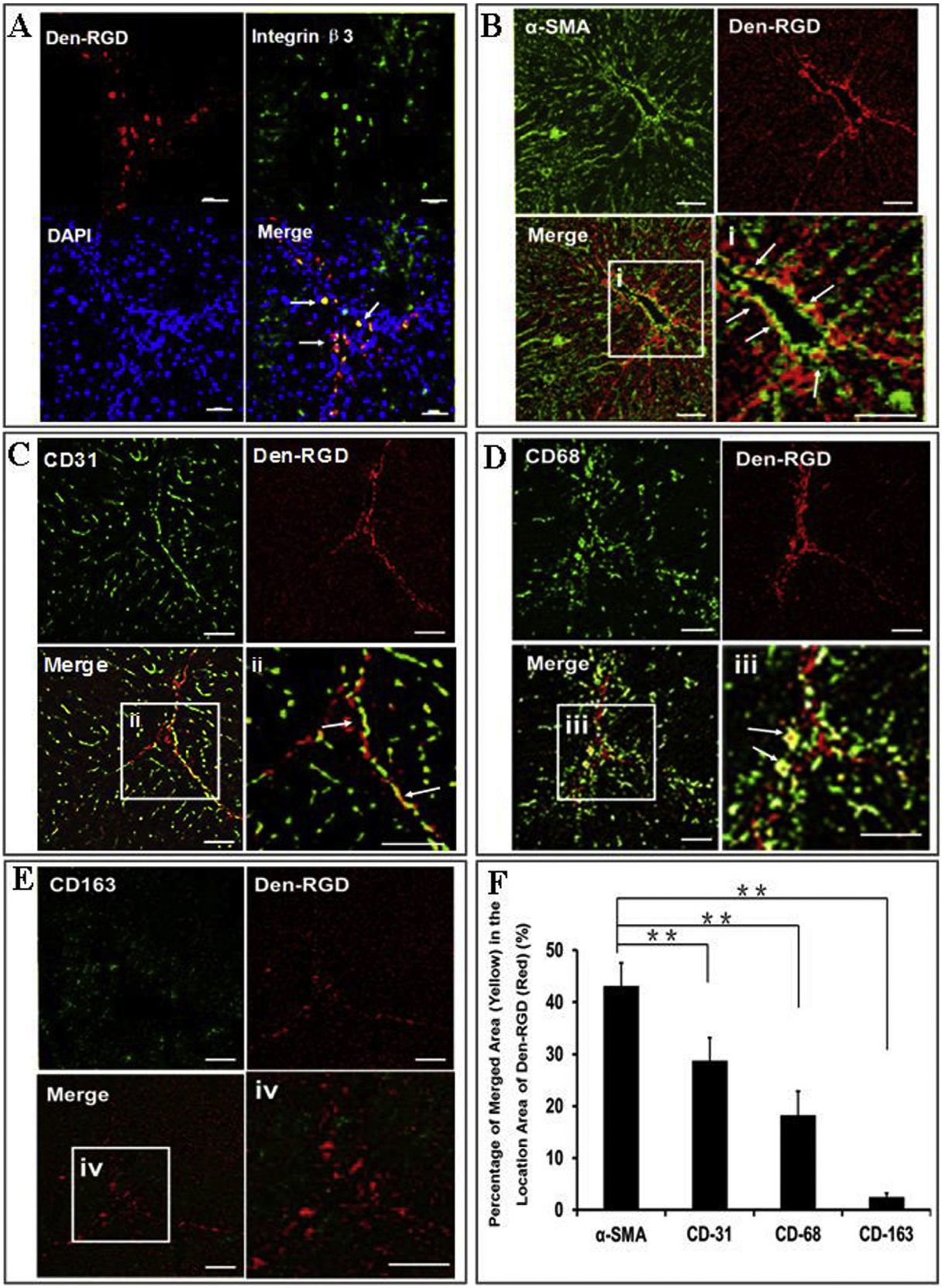

Fig. 8. Localization of Den-RGD nanoprobes in fibrotic livers. (A–E) Representative fluorescent images of Den-RGD nanoprobes localization areas (red), counterstained with β3 integrin subunit (A), α-SMA (B), CD31 (C), CD68 (D) and CD163 (E) antibody (green) from TAA-12w mice. The merged images show the yellow color area pointed by white arrows. Images were recorded at original magnification (400×) and magnified images (zoom 1:1) corresponding to the indicated areas in boxes are presented in i, ii, iii and iv. Scale bars, 100 μm. (**F**) The percentage of overlapped areas in Den-RGD localization areas was compared. $^{**}p < 0.01$. (For interpretation of the references to colour in this figure legend, the reader is referred to the web version of this article.)

the particle surface [15]. Rhodamine was labeled to trace the localization of the nanoprobe in cultured cells and tissue sections because it is easy to be excited under conventional fluorescent microscope. And multiple paramagnetic Gd-DOTA chelators were conjugated to the nanoprobe to achieve a satisfactory T1-weighted relaxivity. Moreover, in the targeted nanoprobe Den-RGD, cRGDyK was labeled to the dendrimer via a PEG linker. The PEG linking smoothed the steric hindrance of the dendrimer to the ligand-receptor binding. And for the whole nanoprobe, the PEG linking also improves its water-solubility, reduces its toxicity and immunogenicity, and inhibits the enzymatic degradation and the phagolysis by the reticuloendothelial system, which may prolong its circulation time and increase its deposition in organs [25]. Additionally, a proper PEGylation ratio in Den-RGD may not only improve the biocompatibility of the nanoprobe, but also reserve the enough conjugation position on the nanocarrier to label sufficient imaging molecules for MRI imaging.

In MTT cell proliferation assay, it was found that with an increase in their concentration, Den-RGD nanoprobes significantly decreased the viability of activated HSCs, whereas Den-PEG nanoprobes didn't have a marked effect. Integrin αvβ3 has been found to bind to the components of ECM, and promotes HSC proliferation and survival [9]. Thus, Den-RGD nanoprobes bound to integrin αvβ3 inevitably interfered with the binding between integrin αvβ3 on the surface of HSCs and ECM, and inhibited HSC viability.

In conclusion, the findings in the present study demonstrate that the deposition of Den-RGD nanoprobes is mainly mediated by cRGDyK which specifically binds to integrin αvβ3 receptors on activated HSCs, and hepatic deposition amount of Den-RGD nanoprobes is markedly increased in parallel with the development and progression of liver fibrosis. Thus, Den-RGD nanoprobes represent as a useful tracer for non-invasively quantitatively assessing the extent of liver fibrosis with an MRI modality.

Financial support

This work was supported by the National Natural Science Foundation of China (Grant NO. 30770970 to Wang J, NO. 81270007 to Li F, NO. 81301875 to Yan H and NO. 81272436 & 81572356 to Wu J), the Nano Science and Technology Projects of Shanghai Science and Technology Commission (Grant NO. 12nm0501400 to Wang J), Shanghai Talent Development Funds (Grant NO. 201304 to Li F), Shanghai Rising-Star Program (Grant NO. 13QA1400700 to Li F) and Shanghai Outstanding Young Talent Training Plan in Health System (Grant NO. 13YO56 to Li F).

Acknowledgements

No.

References

[1] L. Castera, M. Pinzani, Non-invasive assessment of liver fibrosis: are we ready? Lancet 375 (2010) 1419–1420.
[2] L. Castera, P. Bedossa, How to assess liver fibrosis in chronic hepatitis C: serum markers or transient elastography vs. liver biopsy? Liver. Int. 31 (2011) 13–17.
[3] D. Schuppan, Y.O. Kim, Evolving therapies for liver fibrosis, J. Clin. Investig. 123 (2013) 1887–1901.
[4] D.S. Manning, N.H. Afdhal, Diagnosis and quantitation of fibrosis, Gastroenterology 134 (2008) 1670–1681.
[5] N.J. Torok, J.A. Dranoff, D. Schuppan, S.L. Friedman, Strategies and endpoints of antifibrotic drug trials: summary and recommendations from the AASLD emerging trends Conference, Chicago, June 2014, Hepatology 62 (2015) 627–634.
[6] J. Parkes, P. Roderick, S. Harris, C. Day, D. Mutimer, J. Collier, et al., Enhanced liver fibrosis test can predict clinical outcomes in patients with chronic liver disease, Gut 59 (2010) 1245–1251.
[7] J. Vergniol, J. Foucher, E. Terrebonne, P.H. Bernard, B. le Bail, W. Merrouche, et al., Noninvasive tests for fibrosis and liver stiffness predict 5-year outcomes of patients with chronic hepatitis C, Gastroenterology 140 (2011) 1970–1979.
[8] J.S. Desgrosellier, D.A. Cheresh, Integrins in cancer: biological implications and therapeutic opportunities, Nat. Rev. Cancer 10 (2010) 9–22.
[9] X. Zhou, F.R. Murphy, N. Gehdu, J. Zhang, J.P. Iredale, R.C. Benyon, Engagement of integrin αvβ3 regulates proliferation and apoptosis of hepatic stellate cells, J. Biol. Chem. 279 (2004) 23996–24006.
[10] F. Li, Z. Song, Q. Li, J. Wu, J. Wang, C. Xie, et al., Molecular imaging of hepatic stellate cell activity by visualization of hepatic integrin αvβ3 expression with SPECT in rat, Hepatology 54 (2011) 1020–1030.
[11] E. Patsenker, Y. Popov, F. Stickel, V. Schneider, M. Ledermann, H. Sägesser, Pharmacological inhibition of integrin αvβ3 aggravates experimental liver fibrosis and suppresses hepatic angiogenesis, Hepatology 50 (2009) 1501–1511.
[12] E. Patsenker, F. Stickel, Role of integrins in fibrosing liver diseases, Am. J. Physiol. Gastrointest. Liver. Physiol. 301 (2011) G425–G434.
[13] X.W. Huang, J.Y. Wang, F. Li, Z.J. Song, C. Xie, W.Y. Lu, Biochemical characterization of the binding of cyclic RGDyK to hepatic stellate cells, Biochem. Pharmacol. 80 (2010) 136–143.
[14] H. Yan, L. Wang, J. Wang, X. Weng, H. Lei, X. Wang, et al., Two-order targeted brain tumor imaging by using an optical/paramagnetic nanoprobe across the blood brain barrier, ACS. Nano 24 (2012) 410–420.
[15] T. Barrett, G. Ravizzini, P.L. Choyke, H. Kobayashi, Dendrimers in medical nanotechnology, IEEE Eng. Med. Biol. Mag. 28 (2009) 12–22.
[16] J. Zhu, J. Wu, E. Frizell, S.L. Liu, R. Bashey, R. Rubin, et al., Rapamycin inhibits hepatic stellate cell proliferation in vitro and limits fibrogenesis in an in vivo model of liver fibrosis, Gastroenterology 117 (1999) 1198–1204.
[17] K. Ishak, A. Baptista, L. Bianchi, F. Callea, J. De Groote, F. Gudat, et al., Histological grading and staging of chronic hepatitis, J. Hepatol. 22 (1995) 696–699.
[18] S. Liu, Radiolabeled cyclic RGD peptides as integrin alpha(v)beta(3)-targeted radiotracers: maximizing binding affinity via bivalency, Bioconjug. Chem. 20 (2009) 2199–2213.
[19] J.D. Hood, D.A. Cheresh, Role of integrins in cell invasion and migration, Nat. Rev. Cancer 2 (2002) 91–100.
[20] A.S. Chung, Q. Gao, W.J. Kao, Either integrin subunit beta1 or beta3 is involved in mediating monocyte adhesion, IL-1beta protein and mRNA expression in response to surfaces functionalized with fibronectin-derived peptides, J. Biomater. Sci. Polym. Ed. 18 (2007) 713–729.
[21] A.J. Beer, M. Schwaiger, Imaging of integrin alphavbeta3 expression, Cancer. Metastasis. Rev. 27 (2008) 631–644.
[22] S. Singh, S.K. Venkatesh, Z. Wang, F.H. Miller, U. Motosugi, R.N. Low, et al., Diagnostic performance of magnetic resonance elastography in staging liver fibrosis: a systematic review and meta-analysis of individual participant data, Clin. Gastroenterol. Hepatol. 13 (2015) 440–451.
[23] M. Polasek, B.C. Fuchs, R. Uppal, D.T. Schühle, J.K. Alford, G.S. Loving, et al., Molecular MR imaging of liver fibrosis: a feasibility study using rat and mouse models, J. Hepatol. 57 (2012) 549–555.
[24] B.C. Fuchs, H. Wang, Y. Yang, L. Wei, M. Polasek, D.T. Schühle, et al., Molecular MRI of collagen to diagnose and stage liver fibrosis, J. Hepatol. 59 (2013) 992–998.
[25] Y. Kim, A.M. Klutaz, K.A. Jacobson, Systematic investigation of polyamidoamine dendrimers surface-modified with poly(ethylene glycol) for drug delivery applications: synthesis, characterization, and evaluation of cytotoxicity, Bioconjugate. Chem. 19 (2008) 1660–1672.